Porous Copper Microspheres for Selective Production of Multicarbon Fuels via CO₂ Electroreduction

Chengqin Zou, Cong Xi, Deyao Wu, Jing Mao, Min Liu, Hui Liu, Cunku Dong, and Xi-Wen Du*

The electroreduction of carbon dioxide (CO_2) toward high-value fuels can reduce the carbon footprint and store intermittent renewable energy. The iodide-ion-assisted synthesis of porous copper (P-Cu) microspheres with a moderate coordination number of 7.7, which is beneficial for the selective electroreduction of CO_2 into multicarbon (C_{2+}) chemicals is reported. P-Cu delivers a C_{2+} Faradaic efficiency of 78 ± 1% at a potential of −1.1 V versus a reversible hydrogen electrode, which is 32% higher than that of the compact Cu counterpart and approaches the record (79%) reported in the same cell configuration. In addition, P-Cu shows good stability without performance loss throughout a continuous operation of 10 h.

The electrochemical reduction of carbon dioxide (CO_2RR) provides an attractive and viable strategy to produce sustainable chemical fuels,[1,2] meanwhile, this technique is appealing to address the storage of intermittent energy and the release of CO_2.[3] A charming goal for CO_2RR is to produce high-value multicarbon (C_{2+}) chemicals, such as ethylene (C_2H_4), ethanol (C_2H_5OH), acetic acid (CH_3COOH), and n-propanol (C_3H_7OH), which can be achieved with the help of copper (Cu) catalyst. Compared with other catalysts, Cu is the most efficient one for the production of C_{2+} chemicals.[4–7] However, methane (CH_4) and undesired hydrogen (H_2) are usually generated in the presence of Cu catalyst.[8–10] Hence, it is of interest to develop advanced Cu electrocatalysts in favor of the C_{2+} production.

It is widely accepted that CO_2RR on Cu is initiated by reducing CO_2 to adsorbed CO (*CO), and further dimerization of *CO species can lead to C_{2+} products.[11–14] Particularly, CO=CO dimerization exhibits a volcano plot related to the adsorption of *CO, where the optimized adsorption energy,

neither too strong nor too weak, allows easy dimerization.[6,15] Furthermore, the adsorption energies of the intermediates vary with the coordination number (CN) of the catalyst, which can be tuned by the structure of catalysts,[16,17] as such, there also exists a volcano plot between the catalytic activity and CN. Hitherto, the volcano plots have been established for several electrochemical reactions (e.g., oxygen reduction reaction).[16,18] As for CO_2RR, it has been demonstrated that theoretically, moderate CNs between 6 and 8 can promote the CO=CO dimerization on Cu catalyst.[19,20] And experimentally, Cu (100) surface with CN of 8 has been identified as the active site to catalyze *CO intermediate into C_{2+} products.[13,21–23] In contrast, Cu (111) surface with CN of 9 does not favor the CO=CO dimerization.[21,22,24] Nevertheless, practical Cu catalysts with large active surface and moderate CN have not been investigated intensively, and it remains as a great challenge to achieve Cu catalyst with optimized CN for the production of C_{2+} fuels.

Halide ions are known as effective inducing reagents for the synthesis of nanostructured metal due to the strong affinity and adsorption capability.[25–27] As for CO_2RR, Ogura et al. adopted halide to promote the ethylene production at a three-phase interface.[28,29] Recently, Yeo et al. found that the addition of halide ions into electrolyte could improve the current density and selectivity of CO_2RR. In this case, the adsorbed iodide ions were proposed to increase *CO coverage on Cu surfaces, which thus lowers the energy barrier for C–C coupling;[30–32] meanwhile, the catalyst morphology was changed in the presence of iodide ions.[31,32] However, the halide ions have never been utilized to adjust CN of the catalyst and boost the selectivity of CO_2RR.

In this work, we report the synthesis of porous Cu (P-Cu) with moderate CN (7.7) via electroreduction of Cu_2O microspheres in aqueous solution of KI. We demonstrate that the adsorption of iodide ions on the product surface plays a crucial role in the formation of P-Cu. As a CO_2RR catalyst, P-Cu achieves a C_{2+} Faradaic efficiency (FE) of 78%, being 32% higher than that achieved on the compact Cu catalyst. Moreover, P-Cu exhibits a good durability without loss of C_{2+} productivity during 10 h of continuous operation. The high CO_2RR performance was found to originate from the moderate CN of P-Cu according to the X-ray absorption spectroscopy (XAS) analysis.

The starting Cu_2O microspheres were synthesized via a modified precipitation method.[33] Subsequently, P-Cu was

C. Q. Zou, C. Xi, D. Y. Wu, Dr. J. Mao, Dr. H. Liu,
Dr. C. K. Dong, Prof. X.-W. Du
Institute of New Energy Materials
School of Materials Science and Engineering
Tianjin University
Tianjin 300072, China
E-mail: xwdu@tju.edu.cn
Prof. M. Liu
Institute of Super-Microstructure and Ultrafast
Process in Advanced Materials
School of Physics and Electronics
Central South University
932 South Lushan Road, Changsha, Hunan 410083, China

The ORCID identification number(s) for the author(s) of this article can be found under https://doi.org/10.1002/smll.201902582.

**ADVANCED
SCIENCE NEWS**

www.advancedsciencenews.com

NANO · MICRO

small

www.small-journal.com

obtained by the electroreduction of Cu_2O microspheres at −1.1 V versus reversible hydrogen electrode (RHE) for 3 h in the CO_2-saturated electrolyte with 0.05 M KI and 0.05 M $KHCO_3$. For comparison, compact Cu (C-Cu) microspheres were prepared with the same procedure in the electrolyte without KI.

The as-prepared Cu_2O sample comprises many agglomerate particles with size around 700 nm, as revealed by scanning electron microscopy (SEM) and transmission electron microscopy (TEM; Figure S1a–c, Supporting Information). Selected area electron diffraction (SAED) suggests a polycrystalline cubic phase (Figure S1d, Supporting Information), which was confirmed by X-ray diffraction (XRD) pattern (Figure S2, Supporting Information). After electroreduction in the electrolyte with KI, the compact Cu_2O microspheres transform into porous particles as indicated by SEM (**Figure 1**a and Figure S3a–c, Supporting Information) and high-angle annular dark-field scanning transmission electron microscopy (HAADF-STEM) (Figure 1b and Figure S3d, Supporting Information). XRD pattern indicates pure metallic Cu phase without residual oxide (Figure 1c), and an average crystallite size of 4.4 nm is determined by the Scherrer equation (Figure S4, Supporting Information). In contrast, after Cu_2O microspheres being electrochemically reduced in the electrolyte without KI, their structure maintains compact as indicated by SEM (Figure 1d), HAADF-STEM (Figure 1e), and TEM (Figure S5, Supporting Information). XRD analysis indicates that residual oxide coexists with metallic copper in the product (Figure 1f). The phase

constitutions of P-Cu and C-Cu are further verified by the SAED results (Figure S6, Supporting Information). Moreover, energy dispersive spectrum (EDS) mapping shows distinct iodine distribution in P-Cu (Figure S7, Supporting Information).

To understand the formation mechanism of P-Cu, we observed the structure change of big Cu_2O particles with several microns in size (M-Cu_2O, see Figures S8 and S9, Supporting Information). The M-Cu_2O was electrochemically reduced at −1.1 V versus RHE in CO_2-saturated electrolytes with KI or without KI, respectively. As expected, a porous structure could be observed in the presence of KI (Figure S10, Supporting Information), whereas discrete particles formed on the surface of M-Cu_2O in the absence of KI (Figure S11, Supporting Information). Specifically, smooth M-Cu_2O surface became rough after 1 h of electroreduction in electrolyte with KI (Figure S10a,b, Supporting Information), and further transformed into porous structure as the reduction proceeded (Figure S10c,d, Supporting Information). At the same time, the diffraction peaks related to Cu_2O weakened obviously (Figure S12, Supporting Information). Those results imply that the porous Cu structure initiates from the surface of M-Cu_2O and develops inward. In this process, the iodide ions are supposed to adsorb onto both Cu_2O and Cu surface due to strong affinity between Cu_2O/Cu and iodide ions.[34–36] The adsorption of iodide ions can cause a regulation effect, namely, Cu_2O matrix is reduced unevenly, and Cu skeleton grows gradually from surface to internal, leading to the formation of porous Cu structure (**Figure 2**).
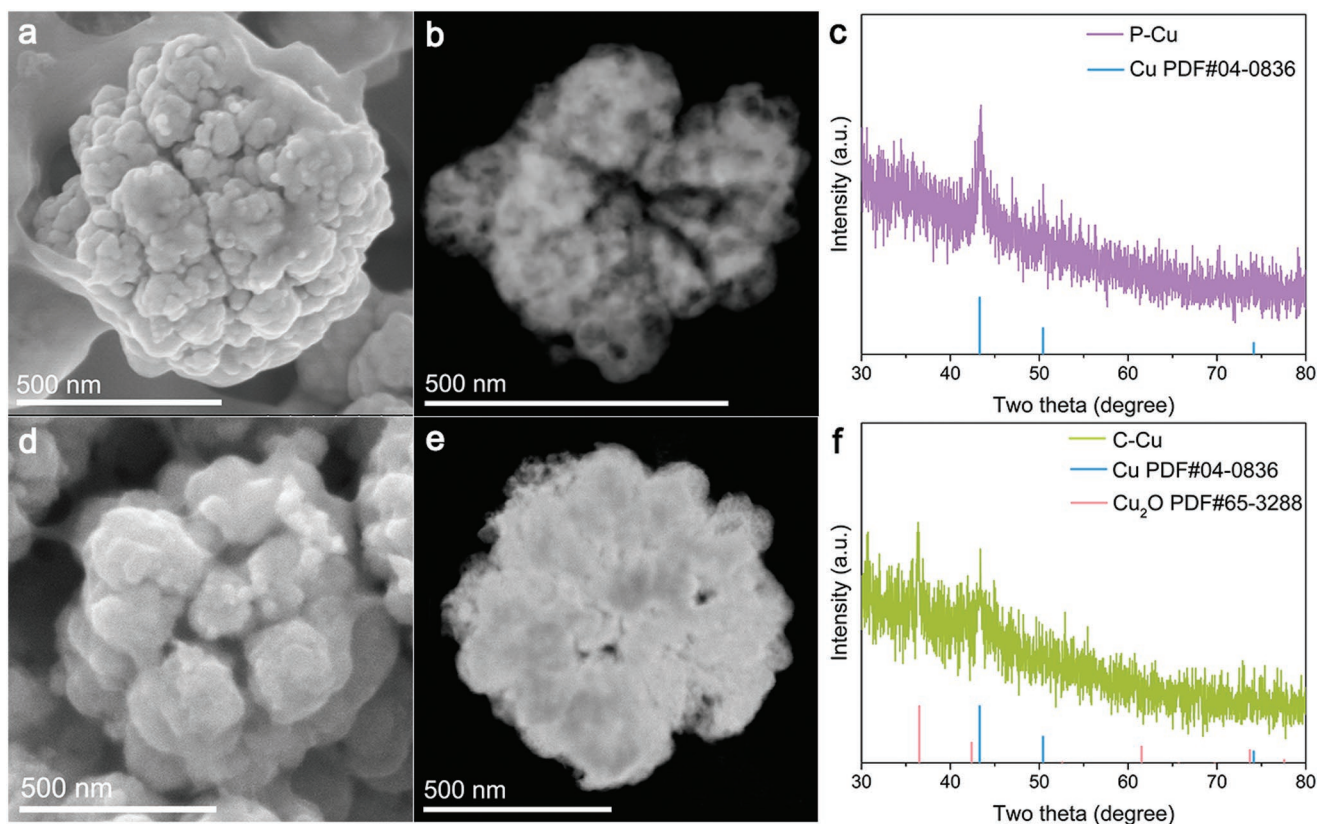

Figure 1. Characterizations of P-Cu and C-Cu. a) SEM, b) HAADF-STEM, and c) XRD of P-Cu obtained in the electrolyte with KI. d) SEM, e) HAADF-STEM, and f) XRD of C-Cu obtained in the electrolyte without KI.
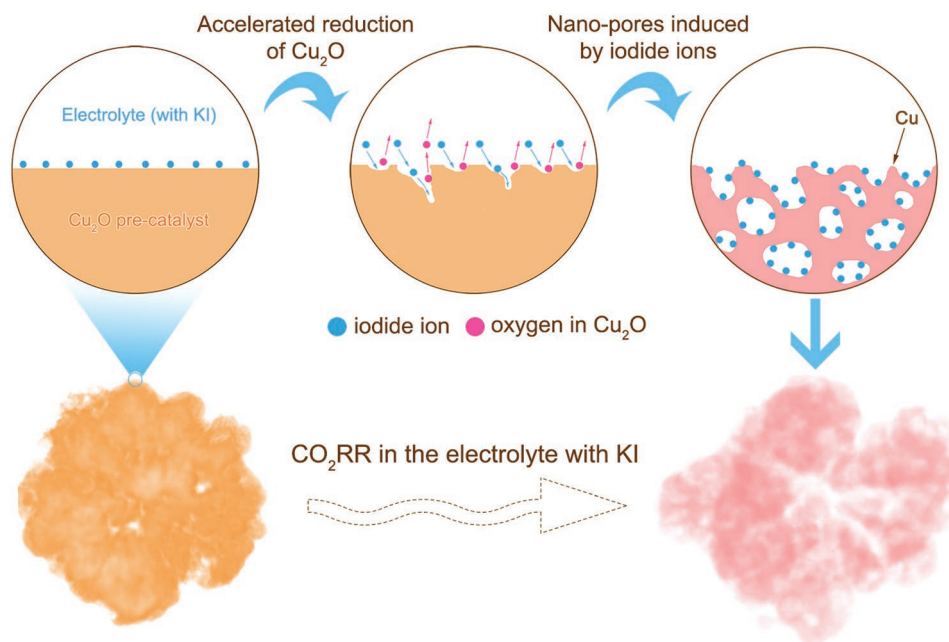
Figure 2. Schematic illustration of the formation mechanism of P-Cu in the presence of iodide ions. The adsorption of iodide ions can promote the uneven reduction of Cu_2O, giving rise to the porous cooper.

This hypothesis was proved by the distribution of iodide ions on P-Cu even after being washed for several times (Figure S7, Supporting Information).

CO$_2$RR performance of the catalysts was evaluated in a H-type electrocatalytic cell (see quantitative methods in the Experimental Section and Figures S13 and S14, Supporting Information). Linear sweep voltammetry (LSV) curves of P-Cu and C-Cu were shown in **Figure 3**a, the geometric current density of P-Cu increases with the applied potential more rapidly than that of C-Cu. Potential screenings demonstrate the optimal C_{2+} (C_2H_4, C_2H_5OH, CH_3COOH, and C_3H_7OH) production can be achieved around −1.1 V versus RHE (Figure S15, Supporting Information). At this potential, the CO$_2$RR current density of P-Cu reaches 46 mA cm^{-2}, whereas the current density of C-Cu is merely 20 mA cm^{-2} (Figure S16, Supporting Information). Based on the evolution of FE(C_2H_4), the activation time for P-Cu was determined as 30 min (Figure S17, Supporting Information). Regarding the CO$_2$RR selectivity at steady states, P-Cu achieves an average FE for C_{2+} (FE(C_{2+})) as high as 78%, including 56% for C_2H_4, 16% for C_2H_5OH, 5% for C_3H_7OH, and 1% for CH_3COOH. By comparison, C-Cu delivers an average FE of 46% for C_{2+}, including 30% for C_2H_4, 13% for C_2H_5OH, 2% for C_3H_7OH, and 1% for CH_3COOH (Figure 3b and Table S1, Supporting Information). For C_{2+} partial current density, P-Cu presents a value four times that of C-Cu (Figure S18, Supporting Information). To exclude the influence of adsorbed iodide ions upon the C_{2+} selectivity, CO$_2$RR performance of P-Cu was evaluated in 0.1 M KHCO$_3$ without KI. Inductively coupled plasma atomic emission spectroscopy (ICP-AES) results demonstrate that the adsorbed iodide ions on P-Cu leach out after working in pure KHCO$_3$ for 1 h (Figure S19, Supporting Information), while no obvious change is found for product constitution and FE(C_{2+}) (Figure S20, Supporting Information). Moreover, the

electrochemical surface area (ECSA) of P-Cu is 2.9 times that of C-Cu according to double-layer capacitance measurements, and the degree of porosity based on ECSA of P-Cu has been improved by four orders of magnitude comparing with that of polycrystalline Cu (Figure S21 and Table S2, Supporting Information). After normalizing the CO$_2$RR current density to ECSA, the intrinsic activity of P-Cu is still higher than that of C-Cu, implying the superiority of porous structure (Figure S22, Supporting Information). P-Cu also shows a good durability, achieving 10 h of continuous operation at −1.1 V versus RHE without loss of performance (Figure 3c). When comparing with literature reported in the H-type electrocatalytic cell, P-Cu manifests a top level of C_{2+} FE, which is comparable with the record (79%) reported so far (Figure 3d and Table S3, Supporting Information). These performance results, taken together, suggest that the porous Cu structure derived in the presence of KI is significant for improving the C_{2+} selectivity in CO$_2$RR.

To understand the specificity of P-Cu, we employed XAS and X-ray photoelectron spectroscopy (XPS) to investigate its composition and structure. The X-ray absorption near edge structures (XANES) at Cu K-edge of P-Cu presents the Cu characteristic peak at ≈9005 eV, while the characteristic peak of Cu_2O is absent at ≈9013 eV, suggesting the complete reduction of Cu_2O microspheres (**Figure 4**a and Figure S23, Supporting Information). Moreover, P-Cu shows a strong peak related to Cu-Cu bond in its R spacing spectrum based on the extended X-ray absorption fine structure (EXAFS) measurements, whereas C-Cu demonstrates a much weaker peak of Cu-Cu bond accompanying with an obvious Cu-O bond. The standard EXAFS fitting reveals that the CNs of P-Cu and C-Cu are 7.7 and 4.9, respectively (Figure 4b and Figure S24 and Table S4, Supporting Information).

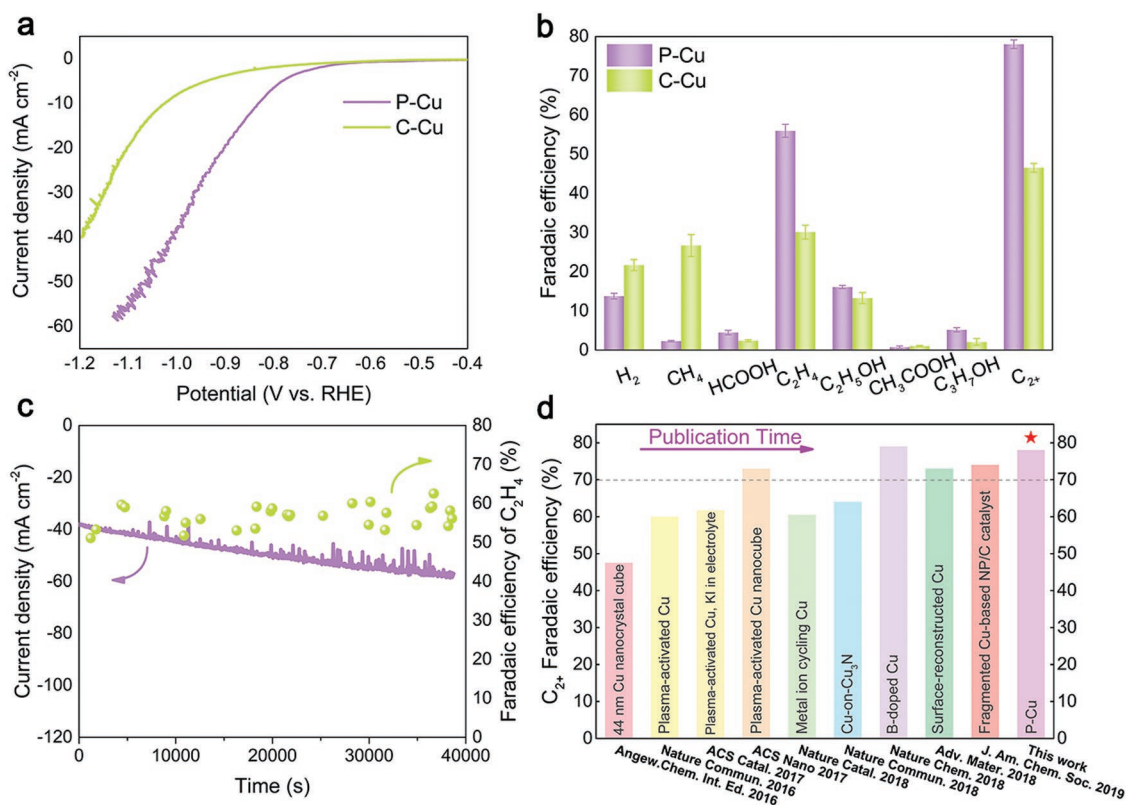In I 3d XPS spectrum of P-Cu, the weak peak at 619.1 eV arises from the adsorbed KI,[37] whose binding energy is

Figure 3. CO$_2$ electroreduction performance of P-Cu and C-Cu. a) LSV scans and b) FEs of different CO$_2$RR products of P-Cu and C-Cu. c) Durability measurement of P-Cu measured at −1.1 V versus RHE. d) Comparison of FE(C$_{2+}$) with literature reported in the H-type electrocatalytic cell. Error bars represent ± standard deviation ($n = 3$ replicates).

distinct from that of CuI (619.7 eV, Figure 4c). Additionally, the XANES at I (iodine) L_{III}-edge of P-Cu does not show any peaks correlating to CuI, but resembles that of KI (Figure 4d). Therefore, both XANES and XPS results imply that iodide ions are adsorbed on the surface of P-Cu, rather than in the form of CuI compound.

It has been reported that the adsorbed iodide ions can improve the CO$_2$RR selectivity of Cu catalysts by strengthening *CO adsorption, enhancing *CO population, and promoting C–C coupling.[29–32] However, iodide ions have never been utilized to adjust CN of the catalyst and boost C$_{2+}$ selectivity of CO$_2$RR. Herein, P-Cu catalyst with an average CN of 7.7 was synthesized with the assistance of iodide ions. As XAS is also bulk sensitive, the average 7.7 of CN for P-Cu suggests there exist lots of low-coordinated surface atoms with CN lower than 7.7, consisting with the small crystallite size of 4.4 nm (Figure S4, Supporting Information) and abundant concave surfaces of P-Cu (Figure 1b and Figure S3d, Supporting Information). Additionally, the absence of iodide in the electrolyte leads to the residual oxide in C-Cu (Figure 1f and Figure S6a, Supporting Information). The residual oxide not only affects the CN of C-Cu, but also causes excessively strong adsorption of CO, which is disadvantageous to the CO=CO dimerization.[38]

In principle, the C$_{2+}$ formation relies on the C–C coupling between two *CO molecules, and the optimized C2 production can be achieved by these catalysts with a moderate adsorption energy for *CO.[6,15] On the other hand, it was verified that the adsorption energy can be tuned by the CN of the catalyst.[19,20] Hence, the catalysts with a moderate CN can optimize the CO=CO dimerization. P-Cu possesses an average CN of 7.7, which just locates in the appropriate CN range of 6–8.[19] Therefore, the high C$_{2+}$ selectivity obtained by P-Cu can be attributed to the appropriate CN of the unique porous nanostructure. Based on the literature,[19,38] a scheme is given in Figure S25 in the Supporting Information to visualize CO$_2$ adsorption and CO=CO dimerization on Cu site with CN = 7 (CN7-Cu): the CO$_2$ molecules are captured and stabilized on the edge CN7-Cu sites with the assistance of H$_2$O molecules adsorbed on neighboring Cu sites by forming hydrogen bonds, while the key intermediates for C$_{2+}$ production, CO dimers, prefer square-like CN7-Cu sites. P-Cu possesses an average CN of 7.7, thus contains abundant surface sites with lower CN (such as CN7-Cu) sites). Hence, P-Cu catalyst is advantageous on the conversion of CO$_2$ to C$_{2+}$ products.

In conclusion, we synthesized porous Cu with a moderate CN for selective multicarbon production in CO$_2$ electroreduction. The porous microspheres were generated by electroreduction of Cu$_2$O microspheres in the electrolyte containing KI, and the adsorption of iodide ions on the surface of Cu$_2$O/Cu was found crucial on the formation of the porous structure. X-ray absorption spectrum indicated that the porous Cu possesses a moderate CN, which is beneficial for the production of multicarbon chemicals. Eventually, the porous Cu catalyst achieves
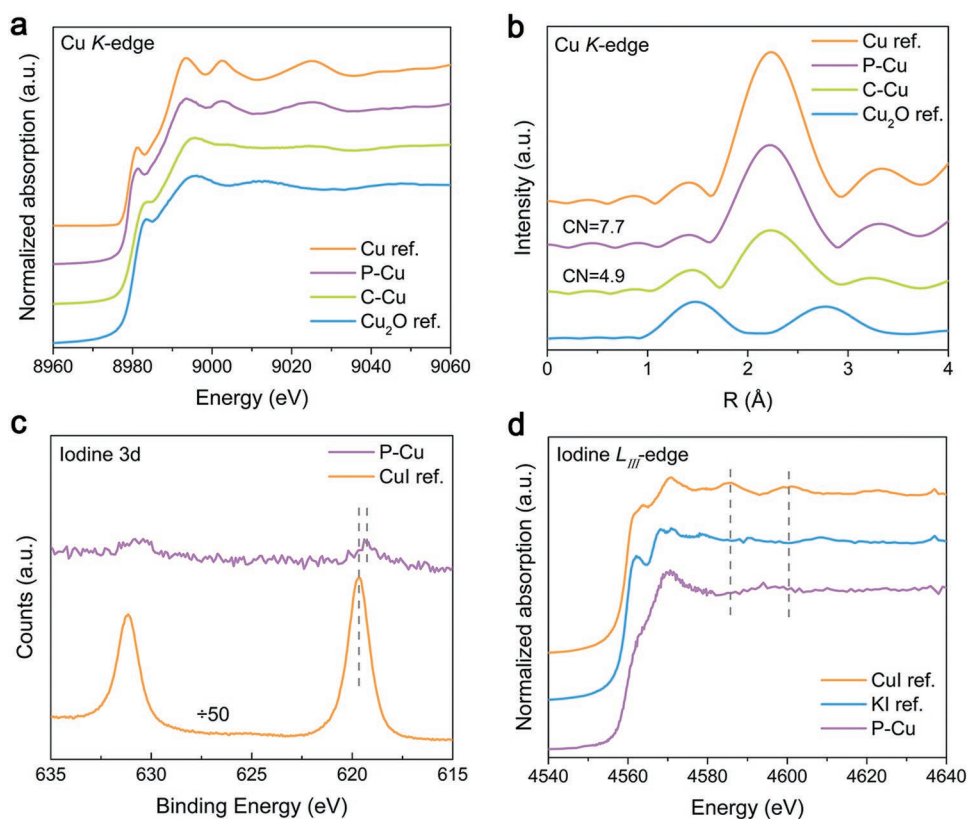
Figure 4. Investigation of the bond structures of P-Cu and C-Cu. a) XANES and b) R-space spectra based on EXAFS of copper at *K*-edge of P-Cu and C-Cu. The commercial Cu₂O and Cu are plotted as references. c) I 3d XPS spectra of P-Cu and the commercial CuI. d) XANES of iodine at *L*ₗₗₗ-edge of P-Cu, the commercial KI, and the commercial CuI.

an FE (78%) of multicarbon product as well as great durability. Our work provides a new avenue toward highly active Cu catalysts for the production of multicarbon chemicals by CO₂ electroreduction.

Experimental Section

Synthesis of Compact Cu₂O: All chemicals were purchased from Sigma-Aldrich. The compact Cu₂O was prepared following a modified precipitation method[33] using cupric acetate monohydrate (Cu(CH₃COO)₂·H₂O), PEG-PPG-PEG (P-123, average Mn ~ 5800), and L-ascorbic acid as precursors. First, 50 mL of 0.1 M Cu(CH₃COO)₂·H₂O was prepared using Millipore water. Next, 1.0 g P-123 and extra 50 mL water were added to the above Cu(CH₃COO)₂·H₂O solution, which was stirred till all P-123 dissolved into the solution. After that, 8 mL of 0.1 M ascorbic acid aqueous solution was quickly injected to the mixed solution, and extra 42 mL water was added with stirring for 1 min. The 150 mL final solution was incubated for 3 h at room temperature. Then, the orange precipitates obtained were subsequently washed four times with 40 mL of water each time and once with 40 mL of acetone to completely remove the unreacted precursors. Finally, the products were obtained by centrifugation and blow-dried using pure N₂.

Characterization: The as-prepared compact Cu₂O pre-catalyst was characterized after preparation. The commercial micro-Cu₂O was characterized as purchased. For the catalysts after reaction, they were obtained after CO₂RR at −1.10 V versus RHE for 3 h. The crystal structures of the samples were characterized with a powder XRD (Bruker D8 Advance) with a copper target (λ = 1.54056 Å). The TEM images, SAED results, HAADF-STEM images, and EDS mapping were collected

on the TEM (JEM-2100F) instrument with an acceleration voltage of 200 kV. SEM (Hitachi S4800, Hitachi SU5000, and FEI Quanta FEG 250) was employed to study the morphology changes. XPS measurements were carried out using a Thermo Scientific K-Alpha system. The binding energy data were calibrated with a reference of carbon C 1s signal at 284.6 eV to correct the charging effect. ICP-AES results were conducted on Optima 7300.

Preparation of Cathode Electrode: The catalyst inks were prepared by ultrasonic dispersing 10 mg Cu₂O pre-catalysts in 1 mL of methanol containing 40 µL of 5 wt% Nafion aqueous solution for 30 min. A glassy carbon electrode (GCE) (diameter: 3 mm, area: 0.07 cm²) that served as a working electrode was used as a substrate to support the catalysts. The samples were prepared by drop-casting 5 µL of the as-prepared inks onto GCE for the subsequent electrochemical measurements.

CO₂RR Performance Evaluation: All CO₂ reduction experiments were performed in a gas-tight two-compartment H-cell separated by a proton exchange membrane (Nafion117) using a three-electrode system. For all experiments, two kinds of electrolytes were used as the catholyte, including 30 mL pure electrolyte without KI (0.1 M KHCO₃) and 30 mL mixed electrolyte with KI (0.05 M KHCO₃ + 0.05 M KI), while anolytes were always 30 mL of 0.1 M KHCO₃. The catholyte was saturated with CO₂, and CO₂ was kept bubbling during the experiments. During CO₂RR test, the activation and performance evaluation of the porous Cu (P-Cu) and the compact Cu (C-Cu) were carried out in the mixed electrolyte with KI and the pure KHCO₃ electrolyte, respectively. Especially for the experiment of P-Cu in the electrolyte without KI (Figure S16, Supporting Information), the P-Cu catalyst was first activated in the electrolyte containing KI, second washed thoroughly with pure water, and finally transferred to the pure KHCO₃ electrolyte for CO₂RR performance evaluation. Pt foil and Ag/AgCl (3 M KCl) were used as the counter electrode and reference electrode, respectively. For potential screenings conducted in 0.1 M

$KHCO_3$ without KI, chronoamperometry measurements were performed at each fixed potential for 3 h in the CO_2-saturated 0.1 M $KHCO_3$. Working electrode potentials were converted to the RHE reference scale using $E_{RHE} = E_{Ag/AgCl} + 0.210 V + 0.0591 \times pH$. All potentials were corrected with 95% of iR correction (the series resistance R was determined using electrochemical impedance spectroscopy). The current densities were normalized to the geometric surface area.

The gas products from CO_2 electroreduction were analyzed using a PerkinElmer Clarus 680 gas chromatograph (GC) coupled with a thermal conductivity detector (TCD) and a flame ionization detector (FID). Gaseous products are separated in a Molecular Sieve 5A capillary column and a Carboxen-1000 packed column, and the TCD is used to quantify CO and H_2, while the FID is used to quantify the hydrocarbons such as CH_4 and C_2H_4. Argon (Linde, 99.999%) was used as the carrier gas.

The FE for gas products was calculated using the following formula

$$FE(\%) = \frac{zFG\rho}{V_m i_{total}} \times 100 \quad (1)$$

where z is the number of electrons transferred, F is Faraday's constant, G is the flow rate of gas, ρ is the molar fraction of the product, V_m is the gas molar volume ($T = 20 °C$, $P = 101.3 kPa$, $V_m = 24 L mol^{-1}$), and i_{total} is the total current.

For molar fraction ρ, it can be calculated using the following formula

$$\rho = \frac{A_x}{\alpha_x} \quad (2)$$

where A_x is the peak area of x product (x could be C_2H_4, CH_4, CO, or H_2) and α_x is the response coefficient of product x in GC. Then, in combination with Formula (2) and Formula (1), the following Formula (3) can be obtained

$$FE(x, \%) = \frac{zFGA_x}{V_m i_{total}\alpha_x} \times 100 \quad (3)$$

Standard gas (C_2H_4, CH_4, CO, or H_2 with CO_2 as the balance gas) was used to make calibration to get the response coefficient α_x. Generally, the calibration of each kind of gas was done with three different concentrations. Here, we take C_2H_4 as an example for GC calibration and FE calculation. First, three different concentrations of 226, 673, and 1111 ppm of standard C_2H_4 gases were injected into GC repeatedly, then three averaged response peak areas of 31 084, 90 502, and 1 44 359 were obtained. Second, plotted the peak area with concentration using ppm as x and peak area as y, and get the slope of 130.01 ppm^{-1} via linear fitting as shown in Figure S13 in the Supporting Information. This slope was the response coefficient α_x of C_2H_4 in GC.

Third, FE of C_2H_4 was calculated by substituting known data into Formula (3). Here, 12, 96 485 $C mol^{-1}$, 20 mL min^{-1}, 24 L mol^{-1}, and 130.01 ppm^{-1} were used to substitute z, F, G, V_m, and α_x, respectively. So, the following Formula (4) can be obtained

$$FE(C_2H_4, \%) = \frac{12 \cdot 96485 \, C \, mol^{-1} \cdot 20 \, mL \, min^{-1} \cdot A_{C_2H_4}}{24 \, L \, mol^{-1} \cdot i_{total} \cdot 130.01 \, ppm^{-1}} \times 100$$
$$= \frac{12 \cdot 96485 \, C \, mol^{-1} \cdot 20 \times 10^{-6} \times 60^{-1} \, m^3 \, s^{-1} \cdot A_{C_2H_4}}{24 \times 10^{-3} \, m^3 \, mol^{-1} \cdot i_{total}(mA) \times 10^{-3}A \cdot 130.01 \times 10^6} \times 100 \quad (4)$$
$$= \frac{A_{C_2H_4}}{i_{total}(mA) \cdot 80.9}$$

For P-Cu, the total current was about 3.2 mA at -1.1 V versus RHE, while the average peak area of C_2H_4 was about 14 500, thus, the FE of C_2H_4 was calculated based on Formula (4) as about 56%.

Regarding the FE for other products, the similar calibration method and calculation method can be applied.

Liquid products were quantified using a Agilent DD2 500 MHz NMR spectrometer. Typically, 500 μL of collected catholyte in the reactor was mixed with 100 μL D_2O containing 30 ppm (n/n) dimethyl sulfoxide (DMSO, ≥99.9%; Sigma-Aldrich) to obtain the internal standard. The 1D ^1H spectrum was measured with water suppression using a pre-saturation method. One typical ^1H NMR spectrum of P-Cu is shown in Figure S14 in the Supporting Information.

As the concentration of DMSO is known, the amount of substance of each liquid product can be calculated based on their relative peak area comparing to that of DMSO. Finally, the FE for liquid products was calculated using the following formula

$$FE(y, \%) = \frac{zFn_{DMSO}\alpha_y v}{\int_0^t i_{total}} \times 100 \quad (5)$$

where z is the number of electrons transferred, F is Faraday's constant, n_{DMSO} is the amount of substance of DMSO used, α_y is the molar ratio of the product y and DMSO based on the NMR peak areas (y could be CH_3CH_2OH, $CH_3CH_2CH_2OH$, HCOOH, or CH_3COOH, whose α_y is equal to the product of the respective relative NMR peak area and 2, 2, 6, or 2, respectively), v is the ratio of total catholyte and the collected catholyte for NMR test, t is the reaction time for collecting liquid products, and i_{total} is the total current.

X-Ray Absorption Experiments: Cu K-edge XANES and EXAFS spectra were performed at the Soft X-ray Microcharacterization Beamline 06B1-1 of Canadian Light Source (CLS). Measurements were performed in fluorescence using a passivated implanted planar silicon detector. IFEFFIT software was used to calibrate the energy scale, to correct the background signal, and to normalize the intensity. The spectra were normalized with respect to the edge height after subtracting the pre-edge and post-edge backgrounds using Athena software. All Fourier transforms were k^2-weighted. EXAFS fittings were conducted at the first shell with Artemis and IFEFFIT software. $S_0/\Delta\sigma^2$ values of 0.83/0.009 for pure Cu model were determined from the Cu K-edge XAS of Cu reference (Cu foil, CN = 12), which were directly applied to the Cu K-edge XAS fittings of P-Cu catalyst. As C-Cu contains residual oxides, one Cu-O model (with one O atom in a $1 \times 1 \times 2$ Cu supercell) and S_0 value of 0.79 were applied to the Cu K-edge XAS fittings of C-Cu catalyst. The detailed fitting results are listed in Table S4 in the Supporting Information.

Supporting Information

Supporting Information is available from the Wiley Online Library or from the author.

Acknowledgements

Conflict of Interest

The authors declare no conflict of interest.

[1] J. Qiao, Y. Liu, F. Hong, J. Zhang, *Chem. Soc. Rev.* **2014**, *43*, 631.

[2] D. D. Zhu, J. L. Liu, S. Z. Qiao, *Adv. Mater.* **2016**, *28*, 3423.

[3] R. W. R. Parker, J. L. Blanchard, C. Gardner, B. S. Green, K. Hartmann, P. H. Tyedmers, R. A. Watson, *Nat. Clim. Change* **2018**, *8*, 333.

[4] Y. Wang, J. Liu, Y. Wang, A. M. Al-Enizi, G. Zheng, *Small* **2017**, *13*, 1701809.

[5] C.-T. Dinh, T. Burdyny, M. G. Kibria, A. Seifitokaldani, C. M. Gabardo, F. P. García de Arquer, A. Kiani, J. P. Edwards, P. De Luna, O. S. Bushuyev, C. Zou, R. Quintero-Bermudez, Y. Pang, D. Sinton, E. H. Sargent, *Science* **2018**, *360*, 783.

[6] Y. Zhou, F. Che, M. Liu, C. Zou, Z. Liang, P. De Luna, H. Yuan, J. Li, Z. Wang, H. Xie, H. Li, P. Chen, E. Bladt, R. Quintero-Bermudez, T.-K. Sham, S. Bals, J. Hofkens, D. Sinton, G. Chen, E. H. Sargent, *Nat. Chem.* **2018**, *10*, 974.

[7] T.-T. Zhuang, Z.-Q. Liang, A. Seifitokaldani, Y. Li, P. De Luna, T. Burdyny, F. Che, F. Meng, Y. Min, R. Quintero-Bermudez, C. T. Dinh, Y. Pang, M. Zhong, B. Zhang, J. Li, P.-N. Chen, X.-L. Zheng, H. Liang, W.-N. Ge, B.-J. Ye, D. Sinton, S.-H. Yu, E. H. Sargent, *Nat. Catal.* **2018**, *1*, 421.

[8] H. Xie, T. Wang, J. Liang, Q. Li, S. Sun, *Nano Today* **2018**, *21*, 41.

[9] Q. Lu, F. Jiao, *Nano Energy* **2016**, *29*, 439.

[10] Y. Hori, *Electrochemical CO₂ Reduction on Metal Electrodes In Modern Aspects of Electrochemistry*, Springer, New York **2008**.

[11] R. Kortlever, J. Shen, K. J. P. Schouten, F. Calle-Vallejo, M. T. M. Koper, *J. Phys. Chem. Lett.* **2015**, *6*, 4073.

[12] E. Pérez-Gallent, M. C. Figueiredo, F. Calle-Vallejo, M. T. M. Koper, *Angew. Chem.* **2017**, *129*, 3675.

[13] J. H. Montoya, C. Shi, K. Chan, J. K. Nørskov, *J. Phys. Chem. Lett.* **2015**, *6*, 2032.

[14] J. H. Montoya, A. A. Peterson, J. K. Nørskov, *ChemCatChem* **2013**, *5*, 737.

[15] X. Liu, J. Xiao, H. Peng, X. Hong, K. Chan, J. K. Nørskov, *Nat. Commun.* **2017**, *8*, 15438.

[16] F. Calle-Vallejo, J. Tymoczko, V. Colic, Q. H. Vu, M. D. Pohl, K. Morgenstern, D. Loffreda, P. Sautet, W. Schuhmann, A. S. Bandarenka, *Science* **2015**, *350*, 185.

[17] F. Calle-Vallejo, D. Loffreda, M. T. M. Koper, P. Sautet, *Nat. Chem.* **2015**, *7*, 403.

[18] D. Wu, C. Dong, H. Zhan, X.-W. Du, *J. Phys. Chem. Lett.* **2018**, *9*, 3387.

[19] H. Li, Y. Li, M. T. M. Koper, F. Calle-Vallejo, *J. Am. Chem. Soc.* **2014**, *136*, 15694.

[20] J. Li, F. Che, Y. Pang, C. Zou, J. Y. Howe, T. Burdyny, J. P. Edwards, Y. Wang, F. Li, Z. Wang, P. De Luna, C.-T. Dinh, T.-T. Zhuang, M. I. Saidaminov, S. Cheng, T. Wu, Y. Z. Finfrock, L. Ma, S.-H. Hsieh, Y.-S. Liu, G. A. Botton, W.-F. Pong, X. Du, J. Guo, T.-K. Sham, E. H. Sargent, D. Sinton, *Nat. Commun.* **2018**, *9*, 4614.

[21] K. J. P. Schouten, Z. S. Qin, E. P. Gallent, M. T. M. Koper, *J. Am. Chem. Soc.* **2012**, *134*, 9864.

[22] K. J. P. Schouten, E. Pérez Gallent, M. T. M. Koper, *ACS Catal.* **2013**, *3*, 1292.

[23] T. Cheng, H. Xiao, W. A. Goddard, *Proc. Natl. Acad. Sci. U. S. A.* **2017**, *114*, 1795.

[24] H. Xiao, T. Cheng, W. A. Goddard, *J. Am. Chem. Soc.* **2017**, *139*, 130.

[25] S. Ghosh, L. Manna, *Chem. Rev.* **2018**, *118*, 7804.

[26] Y. Liu, Y. Xiang, Y. Zhen, R. Guo, *Langmuir* **2017**, *33*, 6372.

[27] Z. Zhang, H. Li, F. Zhang, Y. Wu, Z. Guo, L. Zhou, J. Li, *Langmuir* **2014**, *30*, 2648.

[28] K. Ogura, H. Yano, T. Tanaka, *Catal. Today* **2004**, *98*, 515.

[29] K. Ogura, *J. CO2 Util.* **2013**, *1*, 43.

[30] A. S. Varela, W. Ju, T. Reier, P. Strasser, *ACS Catal.* **2016**, *6*, 2136.

[31] D. Gao, F. Scholten, B. R. Cuenya, *ACS Catal.* **2017**, *7*, 5112.

[32] Y. Huang, C. W. Ong, B. S. Yeo, *ChemSusChem* **2018**, *11*, 3299.

[33] C. Young-Sik, H. Young-Duk, *Bull. Korean Chem. Soc.* **2014**, *35*, 3239.

[34] G. Lefèvre, A. Walcarius, J. J. Ehrhardt, J. Bessière, *Langmuir* **2000**, *16*, 4519.

[35] X. Zhang, P. Gu, X. Li, G. Zhang, *Chem. Eng. J.* **2017**, *322*, 129.

[36] Y. Au, Y. Lin, R. G. Gordon, *J. Electrochem. Soc.* **2011**, *158*, D248.

[37] W. E. Morgan, J. R. Van Wazer, W. J. Stec, *J. Am. Chem. Soc.* **1973**, *95*, 751.

[38] H. Xiao, W. A. Goddard, T. Cheng, Y. Liu, *Proc. Natl. Acad. Sci. U. S. A.* **2017**, *114*, E7045.